eNeuro

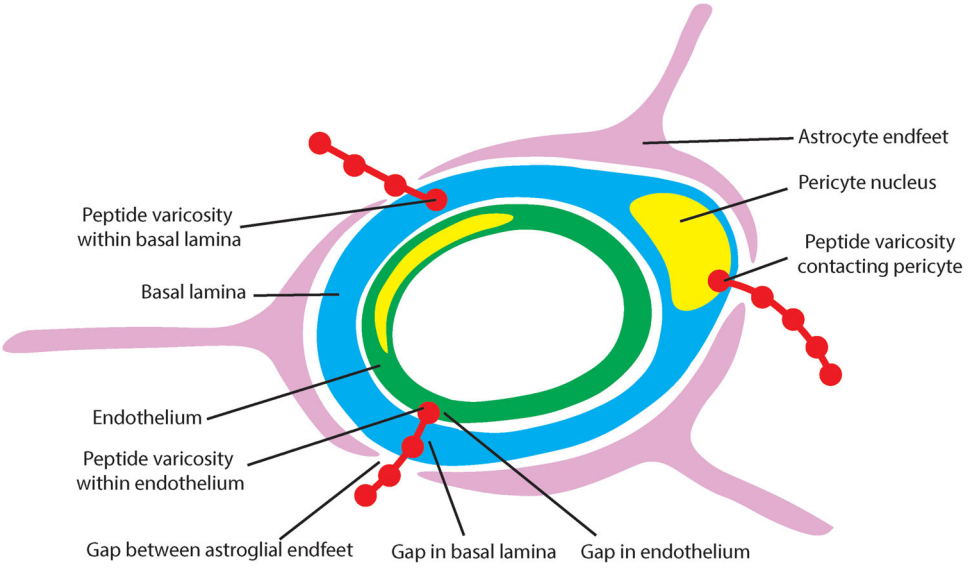
Research Article: New Research
Integrative Systems

Breaching the Blood–Brain Interface: Vasoactive Neurons Contact Capillary Vessels of the Brain Clock in the Suprachiasmatic Nucleus

Yifan Yao,[1] Isabella Cannava,[2] Ruya Tazebay,[3] Saphira Samuels,[3] Emily Silverstein,[2] and Rae Silver[1,2,3,4]

[1]Department of Psychology, Columbia University, New York, New York 10027, [2]Department of Neuroscience and Behavior, Barnard College, New York, New York 10027, [3]Department of Pathology, and Cell Biology, Columbia University, New York, New York 10032, and [4]Zuckerman Institute Affiliate, Columbia University, New York, New York 10027

Visual Abstract



Visual Abstract Legend: The capillary endothelium is surrounded by a basal lamina which has an inner and outer layer. Pericytes lie within the basal lamina between these two layers. Much but not all of the capillary basal lamina is surrounded by astrocytes. Gaps in astrocyte coverage of capillary vessels are loci where vasopressin-, gastrin releasing peptide-, and vasoactive intestinal polypeptide-positive processes access the basal lamina, pericytes and the capillary endothelium.

Received Oct. 22, 2025; revised Dec. 29, 2025; accepted Feb. 16, 2026.

The authors declare no competing financial interests.

Author contributions: Y.Y. and R.S. designed research; Y.Y., I.C., R.T., S.S., E.S., and R.S. performed research; Y.Y., I.C., R.T., S.S., E.S., and R.S. analyzed data; Y.Y. and R.S. wrote the paper.

Widefield microscopy was performed with support from Barnard College. Confocal imaging was performed with support from the Zuckerman Institute's Cellular Imaging Platform. This work was supported by grants from the National Science Foundation (NSF) 1749500 and National Institutes of Health (NIH) R21NS134228 to R.S. and the Beckman Foundation to R.T.

Continued on next page.

Abstract

The suprachiasmatic nucleus (SCN) produces diffusible signals sufficient to sustain circadian locomotor rhythms, although the nature of such signals, their targets, and the pathway whereby such signals may travel is unknown. It is possible that the venous portal veins that connect the capillary beds of the SCN to those of the organum vasculosum of the lamina terminalis (OVLT) provide a vascular pathway whereby signals originating in SCN neurons can reach local targets in the OVLT. Given the presence of the blood–brain interface (BBI) within the SCN, it is unclear how diffusible signals originating in SCN

neurons might access the capillary vasculature of this nucleus. Estimates of astrocyte coverage of capillary vasculature range widely, from 70 to 100%, and furthermore such coverage can change dynamically. In the present study, we investigated whether three vasoactive peptidergic processes found in the mouse SCN, namely, vasopressin, vasoactive intestinal peptide, and gastrin-releasing peptide, might breach the BBI, thereby accessing capillary vessels. Using widefield and confocal imaging, we found neuron-to-capillary contacts between varicosities bearing each of these vasoactive peptides and capillary basal membranes, pericytes, and the endothelia in the mouse SCN of either sex. The findings suggest that all three vasoactive peptides may functionally breach the BBI of the SCN highlighting the importance of understanding how these peptides act on local vasculature to impact blood flow.

Key words: diffusible signal; glymphatic system; neurovascular connection; portal system; vasculature

Significance Statement

The suprachiasmatic nucleus (SCN) produces diffusible signals sufficient to sustain circadian locomotor rhythms. The SCN–organum vasculosum lamina terminalis portal pathway provides a route whereby signals of SCN origin might be relayed to the rest of the brain. The presence of the blood–brain interface (BBI), however, raises the question of how diffusible signals of SCN origin might access the capillary vasculature of the nucleus. High-resolution confocal imaging results suggest that varicosities of vasoactive peptides found in the SCN, namely, vasopressin, vasoactive intestinal peptide, and gastrin-releasing peptide, breach the BBI and directly contact capillary vessel compartments including basal laminae, pericytes, and endothelia.

Introduction

The suprachiasmatic nucleus (SCN) serves as a brain clock, setting the phase of daily oscillation throughout the brain and body. The SCN signals the body via both neural efferents and extrasynaptic, diffusible signals (Ono et al., 2024). While SCN neural efferents have been amply studied, the pathway whereby diffusible neurosecretory signals reach their targets is unknown. Several lines of evidence indicate that diffusible signals are sufficient to sustain rhythms in circadian locomotor (Silver et al., 1996) and in extra-SCN electrical activity (Tousson and Meissl, 2004), but not in endocrine (Meyer-Bernstein et al., 1999).

One pathway whereby diffusible signals can reach their targets is by means of the vasculature, possibly via the portal blood vessels (BVs) linking the capillary beds of the SCN and the organum vasculosum of the lamina terminalis (OVLT; described in mouse, rat, and human; Yao et al., 2021; Roy et al., 2024; Yang et al., Under review). Importantly, in vivo studies show that the direction of blood flow is from the SCN to the OVLT (Roy et al., 2024). The joined capillary beds of the SCN and OVLT are positioned to enable signals of hypothalamic origin to reach local targets without dilution in the systemic blood supply, as occurs in the pituitary portal system (Popa and Fielding, 1930). The vascular organization of the SCN itself has been characterized in both rat and mouse (Ambach and Palkovits, 1975; Yao et al., 2023). The foregoing evidence of a portal vascular pathway from the SCN motivated the current effort to study the relationship between SCN neurons and their capillary blood vessels (BVs) in order to explore how diffusible output signals of the SCN might access local target sites via vascular routes.

Given the presence of the blood–brain barrier (BBB) in the SCN, the question arises as to how secretions of SCN neurons might access the capillary, thereby enabling diffusible signals to communicate time-of-day information to the OVLT. The BBB is a semipermeable membrane that is important in filtering substances exchanged between blood and the brain parenchyma (Wu et al., 2023). The anatomical components of the BBB include the BV endothelium, the tight and adherens junctions joining the endothelial cells, the basal lamina surrounding the endothelium, and the pericytes lying within the basal lamina. More recent understanding of the interface between brain and vasculature [i.e., blood–brain interface (BBI)] includes the concepts of the neurovascular unit, transporters, barrier cell secretions, adaptation, and modification of BBB functions (Banks, 2016). The best understood vasoactive peptides include the vasoconstrictor arginine vasopressin (AVP), and the vasodilators, vasoactive intestinal polypeptide (VIP) and gastrin-releasing peptide (GRP; Goadsby and MacDonald, 1985; Goldsmith, 1987; Clive et al., 2001), and these are abundant in the SCN (Moore et al., 2002). Each of these peptides has been implicated as

Correspondence should be addressed to Rae Silver at rae.silver@columbia.edu.

Copyright © 2026 Yao et al.
This is an open-access article distributed under the terms of the Creative Commons Attribution 4.0 International license, which permits unrestricted use, distribution and reproduction in any medium provided that the original work is properly attributed.

an SCN diffusible output (Tousson and Meissl, 2004; Maywood et al., 2011). Furthermore, direct innervation of capillaries by AVP, GRP, and VIP in extra-SCN brain regions has been reported (Uddman et al., 1983; Jójárt et al., 1984; Paspalas and Papadopoulos, 1998). Neurons and their efferents bearing these peptides are spatially organized within the SCN. VIP neurons lie in the core region, AVP neurons lie in the shell, and GRP neurons are localized in a "cap" between the core and shell (Moore and Silver, 1998; Abrahamson and Moore, 2001; Moore et al., 2002). Fibers of these neurons are also spatially organized. AVP fibers lie predominantly in the shell. GRP fibers are densest in the cap and core regions. VIP fibers extend throughout the entire SCN.

Astrocytes and BVs are also spatially organized within the SCN. Glial fibrillary acidic protein-labeled astroglial processes in rat SCN are concentrated in the central area and weaker at rostral and caudal aspects, and some, but not all SCN neurons, are engulfed by astroglial processes (Tamada et al., 1998). With respect to BVs, whole BV length density, capillary length density, and surface area density are significantly greater in the shell than the core (Yao et al., 2023).

In the present study, we sought to determine whether AVP-, VIP-, and GRP-containing neurons innervate SCN capillaries. To this end, we surveyed the SCN using high-resolution confocal imaging of mouse brains labeled with AVP; VIP; GRP; two markers of the SCN vasculature, namely, basal lamina and endothelium; and DAPI for nuclei.

Materials and Methods

Animal and housing. C57BL/6NJ mice from The Jackson Laboratory aged 8–10 weeks were bred in the laboratory. All animals were provided with *ad libitum* access to food and water. The room was maintained at 21 ± 2°C and 35–70% humidity with a 12 h light/dark cycle (lights-on at 7:00 A.M.). All experiments were carried out in accordance with Columbia University's Institutional Animal Care and Use Committee protocol number AC-AABH1603.

Perfusion protocol. Animals were deeply anesthetized (11% ketamine + 2% xylazine, 10 ml/kg body weight, i.p.) and perfused intracardially with 50 ml of 0.9% saline followed by 100 ml of 4% paraformaldehyde (PFA) in 0.1 M phosphate buffer at pH 7.3. Brains were postfixed at 4°C overnight and then cryoprotected in 20% sucrose until sectioning.

Preparation of sections. For sectioning, the brains were embedded 6% and then 12% gelatin solution at 37°C for a minimum of 30 min. Once infiltrated with the gelatin, the brains were hardened at 4°C for at least 2 h. Next, the tissue was further hardened overnight in a solution of 4% PFA and 20% sucrose. Sagittal sections (50 µm) were cut on a cryostat (Leica Biosystems) and collected in 0.1 M phosphate-buffered saline (PBS). After washing in 0.1 M PBS 0.1% Triton X-100, sections were blocked with 1% normal donkey serum 0.1 M PBS 0.3% Triton X-100 for 1 h.

Immunohistology. In order to identify SCN vasoactive neurons and their processes, antibodies to AVP, GRP, and VIP were used as follows: anti-AVP (rabbit, ImmunoStar, catalog #20069, lot #1922002), anti-VIP (rabbit, ImmunoStar, catalog #20077, lot #2006001), and anti-GRP (rabbit, ImmunoStar, catalog #20073, lot #1420001). In order to identify SCN BVs, Type IV Collagen-UNLB antibody (goat, SouthernBiotech, catalog #1340-01, lot #H2915-PI54) was used to label the basal lamina, and tomato lectin fluorescence (Vector Labs, catalog #FL-1171-1, lot #ZK0505) was used to label the endothelium. The following secondary antibodies were used: for AVP, VIP, and GRP, donkey anti-rabbit Cy3 (Jackson ImmunoResearch, code #711-165-152, lot #165051), and for collagen, donkey anti-goat Cy5 (Jackson ImmunoResearch, code #705-175-147, lot #160572). For each antibody, a dilution series was conducted to optimize the working concentration. The best signal-to-noise ratio was anti-AVP at 1:2,500, anti-VIP at 1:1,000, anti-GFP at 1:1,000, anti-collagen at 1:100, and lectin at 1:100. All primary antibodies were incubated with secondary antibodies at 1:200.

Antibody validation was performed using the following approaches. A primary-antibody-free control at each dilution tested was conducted to optimize the working concentration. No staining was observed in the absence of primary antibodies under any dilution. Antibody specificity was further assessed using preadsorption tests, by saturating antibodies with their corresponding antigens according to the manufacturer's instructions. Tissues incubated with antigen-preabsorbed antibodies showed no staining. Finally, the staining patterns observed in the present study are identical to those reported in the published literature (Härtig et al., 2009; Lokshin et al., 2015; Varadarajan et al., 2018; Michalski et al., 2020; Taub et al., 2021).

Microscopy and image processing. For widefield imaging, a Nikon Eclipse Ti2-E equipped with an Andor Zyla Plus sCMOS 4.2 MP USB-3 (water-cooled) and the following filters were used: Ex395/25 Dm425 Bar460/50 DAPI, Ex470/40 Dm495 Bar525/50 FITC/GFP, Ex545/25 Dm565 Em605/70 CY3, and Ex620/60 Dm660 Bar700/75 CY5. Capillaries were defined as BV segments of diameters smaller than 10 µm (Stefanovic et al., 2008) and neural varicosities as swollen elements along a fiber (~0.5–2.5 µm; Ueda et al., 1983; Jacomy et al., 1999).

Next, the regions of interest were imaged with confocal microscopy. For confocal imaging, a SoRa-W1 Yokogawa spinning disk confocal microscope equipped with two Hamamatsu ORCA-Fusion sCMOS cameras and a 63× 1.46 NA Alpha Plan-Apochromat objective (Intelligent Imaging Innovations). Images were reconstructed in 3D with Imaris ver10.2 (Bitplane).

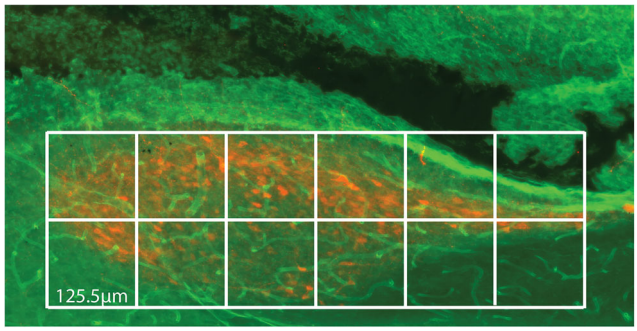


Figure 1. The SCN was compartmentalized into distinct units so as to divide the nucleus into squares of 125.5 × 125.5 µm^2. Each square was examined for contacts of peptide varicosities with the capillary wall.

Quantification. The following numbers of animals were studied for each peptide: AVP $N = 6$ (three females, three males), GRP $N = 4$ (three females, two males), and VIP $N = 7$ (two females, five males). SCN capillary vessels and AVP, VIP, and GRP peptidergic fibers are not uniformly distributed in the SCN. In order to assess the entire extent of the SCN, it was imaged in the sagittal plane using a 20× 0.75 NA CFI Plan Apo Lambda objective. *z* stacks were used to generate an extended depth of focus (EDF) image. To systematically survey the SCN, an image of the nucleus was overlaid with a grid of squares (125.5 × 125.5 µm^2 squares, Fig. 1), and two independent investigators examined an EDF image of each square in the grid for potential points of contact between varicosities and capillary vessels. Each of these regions of interest was then imaged with confocal microscopy. The number of confocal stacks imaged was 62 for AVP, 39 for GRP, and 70 for VIP.

Results

We first asked whether AVP, VIP, and GRP contacts with blood vessels are localized to distinct areas within the volume of the nucleus. The results indicate that processes of AVP, VIP, and GRP neurons contact capillary vessels wherever their fibers and varicosities are located, in both shell and core regions of the SCN. Varicosities of each of the peptidergic types make appositions with three distinct BV wall compartments, namely, the basal lamina matrix, the pericytes (identified by a DAPI-labeled nucleus), and the endothelium (Figs. 2–10). The figures present representative examples of AVP appositions (Figs. 2–4), followed by those of GRP (Figs. 5–7) and VIP (Figs. 8–10) in turn. For each of the vasoactive peptides, we present a set of three figures showing the following results: a varicosity within the basal lamina matrix, a varicosity contacting a presumed pericyte (based on its location within the basal lamina), and finally, a varicosity within the endothelium.

Figures 2–10 are similarly organized. Detailed descriptions of each result are provided in the figure legends. In each figure, Panel A shows a sagittal view of the SCN and indicates the location of the varicosity that is described in detail in the remaining panels (Fig. 9*A* applies to both Figs. 9, 10). Panel B is a higher magnification image of the boxed area in Panel A and shows the dense arrangement of fibers coursing over blood vessels in the region of interest. Subsequent images identify the contact site in increasingly higher resolution images of the varicosity of interest and blood vessel compartments in all three axes (Figs. 2–9*C*,*D*, 10*A*,*B*). To facilitate the visualization of the contact site, each layer of the highest resolution confocal image is traced to make a diagram (Figs. 2–9*E*, 10*C*) using Illustrator (Adobe). In the final images, the pathway of the fiber process that gives rise to the varicosity of interest is shown in a series of confocal images in *z* stacks. This is done by tracking the fiber as it courses toward the capillary vessel. In some cases (Figs. 2, 4, 5, 8), the fiber is en passant while in other cases it terminates at the point of contact with a BV compartment. It is noteworthy that in each case, fibrous varicosities access compartments within capillary vessels at points where there are gaps between astrocytic end feet. These occur at points where collagen staining is much reduced or absent (Figs. 2, 6, 7*D*).

Discussion

Historically, it has been suggested that the BBB acts as a "physical barrier" because of the tight junctions between adjacent endothelial cells (Abbott et al., 2006). Also, brain capillaries are thought to be surrounded by, or closely associated with, the end feet of astrocytes which creates an additional barrier. In the current study, we raise the possibility that the varicosities of all three vasoactive peptides in the SCN access the basal membrane and endothelium indicating that there are gaps in the astrocytic coverage of capillary vesicles.

Astrocytic end feet are a component of the BBB. The experimental evidence in the literature on the extent of coverage and on the frequency of direct contacts between astrocytes and brain blood vessels ranges surprisingly widely, from 70 to 100%. In some estimates, astrocyte end feet outside the basement membrane are said to surround ∼85% of the surfaces of brain capillaries (Bai and Zhou, 2017; Al-Huthaifi et al., 2024). Electron microscopy (EM) in humans showed that the

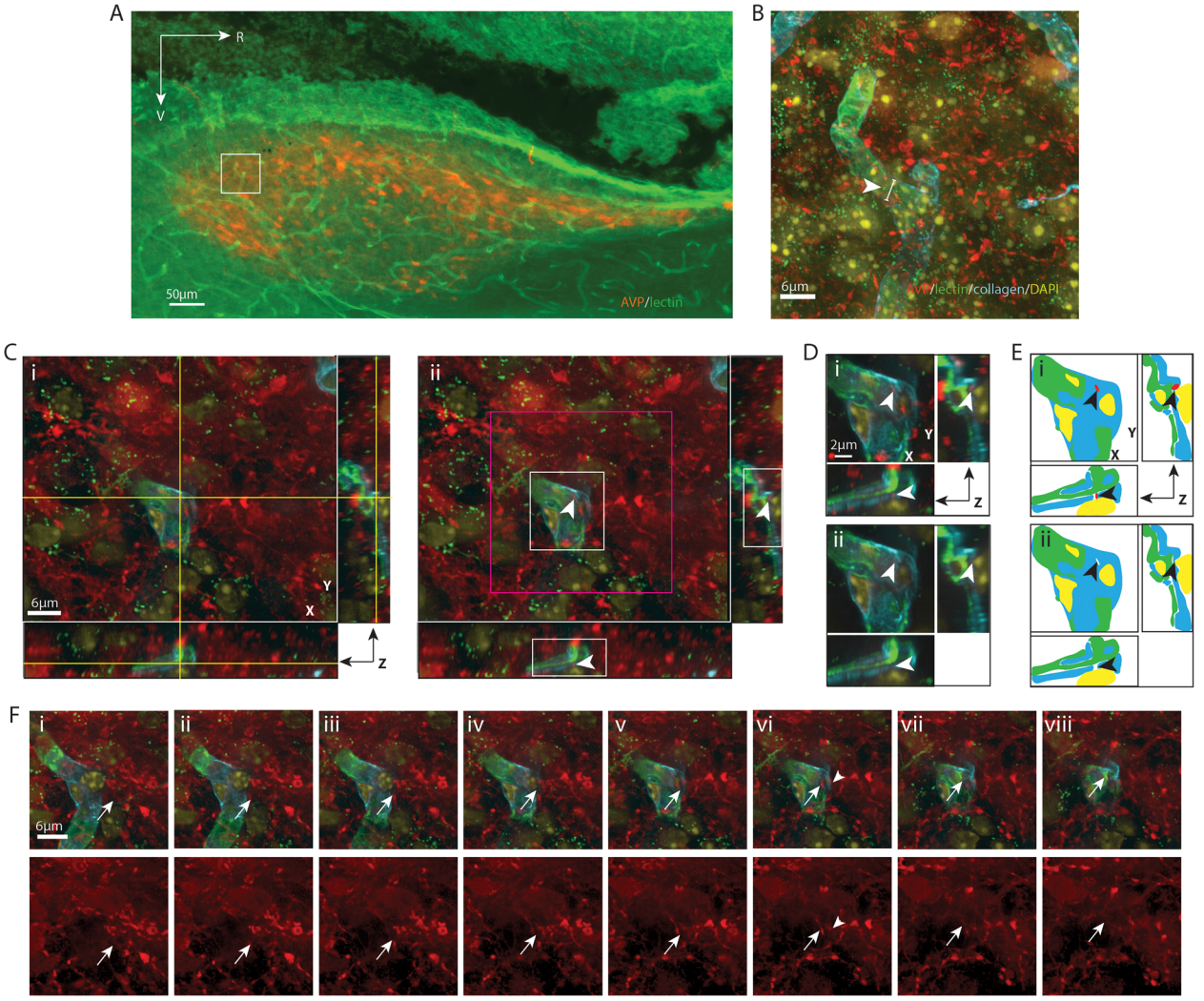


Figure 2. AVP varicosity lying in the capillary basal lamina matrix. ***A***, EDF image of the SCN in sagittal orientation. The boxed area is further examined using confocal microscopy in ***B–F***. The SCN is identified by AVP neurons, and the vascular endothelium is labeled with lectin. ***B***, Maximum intensity projection confocal image of the boxed area in ***A*** with additional labels for basal lamina (collagen) and nuclei (DAPI). AVP-positive fibers are seen coursing over a BV. The capillary segment (arrowhead), examined in the following panels, has a diameter of 5.05 µm. ***C***, An AVP-positive varicosity lying in the basal lamina is shown in all three orientations in an optical section. ***i***, The crosshair overlies the varicosity in the basal lamina. ***ii***, The crosshair is removed to enhance visualization of the varicosity (arrowhead), which has a diameter of 0.72 µm. Higher magnification images of the white and magenta boxed areas are further examined in ***D*** and ***F***, respectively. ***D***, To visualize the varicosity lying within the vascular wall, a magnified view of its localization is shown in three orientations. ***i***, AVP, collagen, lectin, and DAPI staining are merged to show that the varicosity (arrowheads) is in the basal lamina, residing at a curvature point of the capillary segment, and without penetrating into the endothelium layer. ***ii***, Removal of AVP reveals a gap (arrowheads) in the collagen staining where the varicosity resides. ***E***, Cartoon provides an illustration of key elements in ***D***. ***F***, Serial optical sections show the pathway of an AVP fiber (arrows) above (***i–v***) and below (***vii***, ***viii***) a varicosity (***vi***) described in the boxed area in ***C*** as it enters and exits the basal lamina. Top row, Four channels are merged to show the relationship between the fiber and BV wall. Bottom row, The AVP-only channel improves visualization of the fiber. ***i–iv***, A varicosity on the AVP-positive fiber appears. ***iii***, ***iv***, This fiber runs upward in the 11 o'clock direction. ***v***, ***vi***, The fiber branches and runs in the 2 o'clock direction. It penetrates the basal lamina. ***vii***, ***viii***, The fiber exits the BV wall. The arrowhead in ***vi*** serves as a location marker and points to the varicosity seen in ***C*** and ***D***. Color coding: AVP, red; lectin, green; collagen, blue; and DAPI, yellow. AVP, vasopressin; BV, blood vessel; EDF, extended depth of focus; SCN, suprachiasmatic nucleus. For ***B***, $z = 15.1$ µm; for ***C***, ***D***, and ***F***, $z = 0.1$ µm. ***F*** was taken every fourth section along the z stack.

capillary coverage by glia is 85.15 ± 14.37% (Bertossi et al., 1997). Pardridge (2002) commented that >99% of the brain surface of the capillary basement membrane is surrounded by astrocyte end feet processes with occasional neuronal innervation of the capillary. In a study using 3D reconstruction of a small volume of the rat hippocampal CA1 region, based on EM data, Mathiisen et al. (2010) (Fig. 2*C*) reported that there are clefts between astrocytic end feet and suggested that 1% of the pericytes in microvessels are free of astrocyte coverage. The BBB is modulated by pericytes lying in the basal membrane abluminal to the endothelium, and signaling from pericytes regulates the number of tight junctions between endothelial cells (Armulik et al., 2010). The permeability of BBB is impacted by all its components and their interaction with neurons and immune cells (Zhao et al., 2022). Of course, coverage of BV by astrocytes may be regionally differentiated, and astrocytes themselves are very diverse (Haim and Rowitch, 2017). These authors noticed small spaces in the

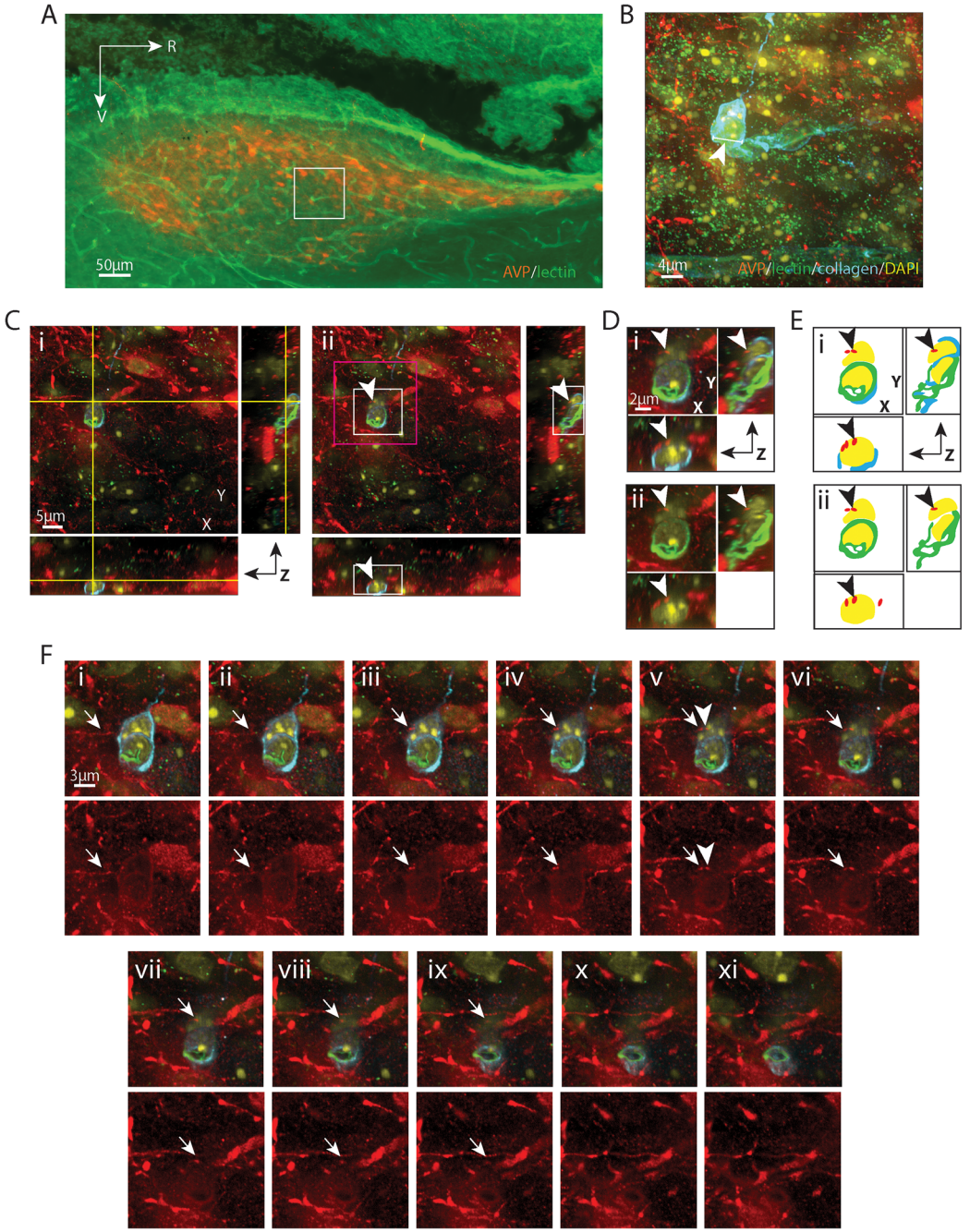


Figure 3. AVP varicosity contacting a pericyte nucleus. ***A***, EDF image of the SCN in sagittal orientation, labeled with AVP for SCN and lectin for endothelium. The boxed area is further examined with confocal microscopy in ***B–F***. ***B***, Maximum intensity projection of confocal image of the boxed area in ***A*** with additional labels of basal lamina (collagen) and nuclei (DAPI). Multiple AVP fibers are seen in close apposition to a capillary. The capillary segment (arrowhead), examined in the following panels, has a diameter of 5.79 µm. This segment is localized at the border between the core and the shell. ***C***, An AVP-positive varicosity, shown in all three orientations, contacts a DAPI-labeled nucleus in an optical section. ***i***, The crosshair denotes the location of a varicosity contacting the DAPI-labeled cell nucleus in the basal lamina. ***ii***, Removal of the crosshair enables better visualization of the varicosity (arrowhead), which has a diameter of 0.61 µm. Higher magnification images of the white and magenta boxed areas are further examined in ***D*** and ***F***, respectively, in order to follow the path of the fiber. ***D***, A magnified view in three orientations of a varicosity contacting the cell nucleus enables better visualization of the varicosity at the point where it contacts the BV wall. ***i***, AVP, collagen, lectin, and DAPI staining are merged to show that the varicosity is in the basal lamina. ***ii***, Removal of collagen shows that the top part of the DAPI-labeled nucleus contacts the AVP-positive varicosity and that its ventral aspect is covered by lectin labelled endothelium. Arrowheads point to the location of the varicosity as in ***C***. ***E***, Cartoon provides traces of key elements in ***D***. ***F***, Serial sections indicate the pathway of an AVP fiber (arrows) coursing above (***i–iv***) and below (***vi–xi***) a varicosity (***v***) that terminates in the basal lamina of the BV wall. Top row, Four channels are merged to show the relationship between the fiber and the cell in the basal lamina. Bottom row, The AVP-only channel allows better visualization of the pathway of the fiber. ***i–iv***, An AVP fiber reaches the capillary and enters the basal lamina. ***v***, The terminal of the AVP fiber contacts a DAPI-labeled nucleus surrounded by collagen. ***vi–ix***, the AVP-positive varicosity and the DAPI-stained nucleus gradually disappear together (***x***, ***xi***). The arrowhead in *v* serves as a location marker and points to the varicosity seen in ***C*** and ***D***. For ***B***, $z = 16.02$ µm; for ***C***, ***D***, and ***F***, $z = 0.06$ µm; ***F*** was taken every fourth section across the *z* stack. Remaining color coding and abbreviations as in Figure 1.

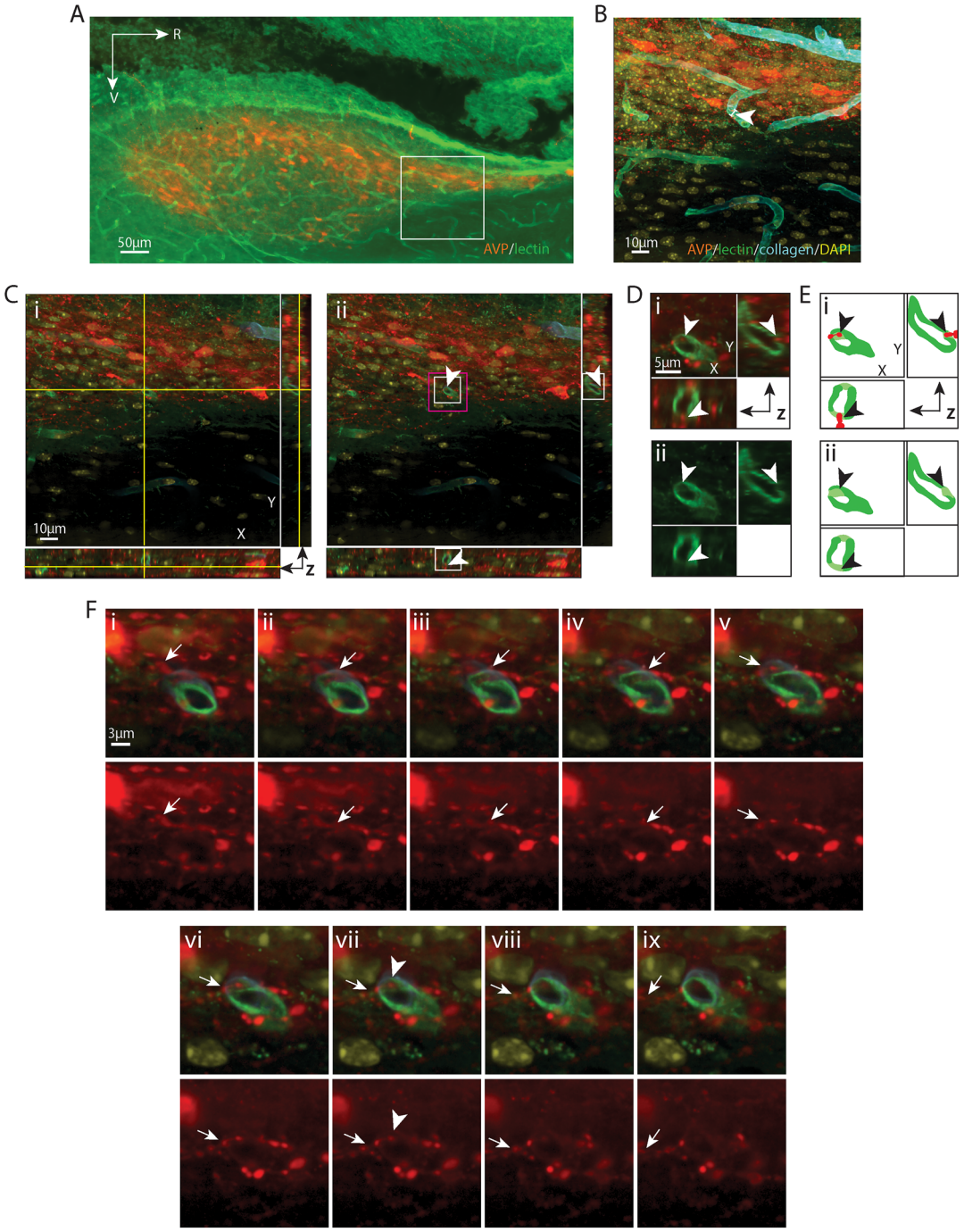


Figure 4. AVP varicosity lying in the capillary endothelium. ***A***, EDF image of the SCN in sagittal orientation, labeled with AVP for SCN and lectin for endothelium. The boxed area is further imaged with a confocal microscope in ***B–F***. ***B***, Maximum intensity projection of confocal image of the boxed area in ***A*** with additional labels of basal lamina (collagen) and nuclei (DAPI). The fibers and cell bodies of AVP neurons are seen entangled with capillaries. The capillary segment (arrowhead) examined in the following panels has a diameter of 6.59 µm. ***C***, An AVP-containing varicosity in the endothelium is shown in all three orientations (same area shown in B). ***i***, The crosshair denotes the location of the varicosity in the endothelium. ***ii***, Removal of the crosshair allows better visualization of the varicosity (arrowheads), which has a diameter of 1.13 µm. Higher magnification images of the white and magenta boxed areas are further examined in ***D*** and ***F***, respectively, in order to follow the path of the fiber. ***D***, Magnified view of the varicosity in all three orientations allows better visualization of the varicosity in relation to the vascular endothelium. ***i***, AVP and lectin staining are merged showing that the varicosity (arrowheads) is in the endothelium. ***ii***, The lectin-only channel shows a gap in lectin staining (arrowheads) where the varicosity resides, seen most clearly in the *xz* and *yz* planes. ***E***, Cartoon provides traces of key elements in ***D***. ***F***, Serial sections indicate the pathway of an AVP fiber (arrows) above (***i–vi***) and below (***viii–ix***) a varicosity (***vii***) which penetrates the endothelium. Top row, Merged images of AVP and BV showsthe pathway of the fiber. Bottom row, The AVP-only channel better displays the fiber. Arrows indicate the path of the fiber. ***i–iv***, A fiber crosses the collagen labeled basal lamina but does not yet access the endothelium at this point. ***v***, ***vi***, A varicosity of this AVP fiber lies close to the endothelium. ***vii***, The varicosity is seen in the endothelium. ***viii***, ***ix***, ***ix–xi***, The fiber exits the endothelium. The arrowhead in ***vii*** serves as a location marker and points to the varicosity seen in ***C*** and ***D***. Color coding and abbreviations as in Figure 1. For ***B***, $z = 18.1$ µm; for ***C***, ***D***, and ***F***, $z = 0.1$ µm; ***F*** was taken from every fourth section in the *z* stack.

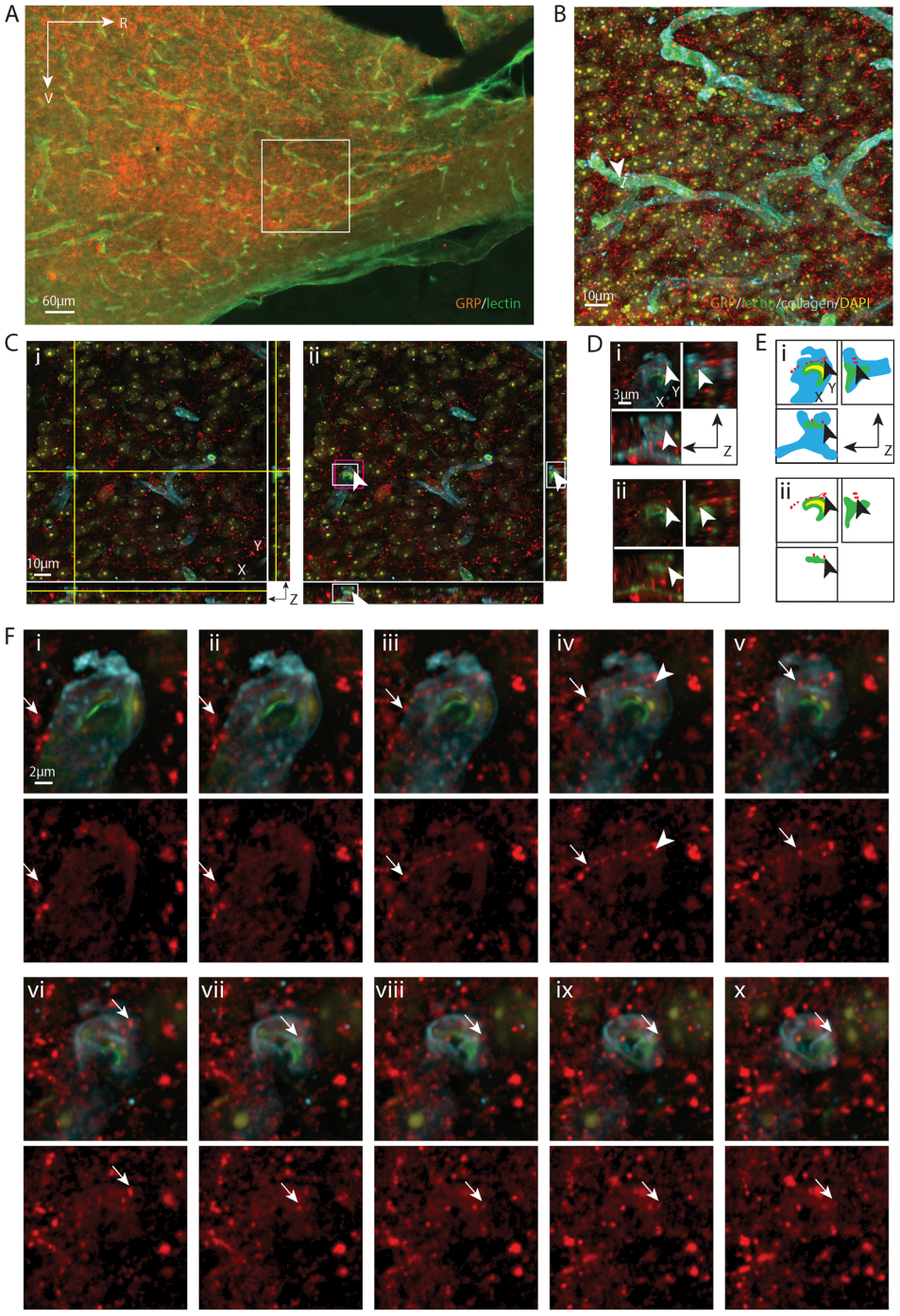


Figure 5. GRP varicosity lying in the capillary basal lamina matrix. ***A***, EDF image of the SCN in sagittal orientation, labeled with GRP for SCN and lectin for endothelium. The boxed area is further examined with confocal microscopy in ***B–F***. ***B***, Maximum intensity projection confocal image of the boxed area in ***A*** with additional labels of basal lamina (collagen) and nuclei (DAPI). Numerous GRP-positive fibers are seen coursing over the BV. The capillary segment (arrowhead) examined in the following panels has a diameter of 8.25 µm. ***C***, A GRP-positive varicosity lying in the basal lamina, shown in all three orientations, in an optical section taken from ***B***. ***i***, The crosshair denotes the varicosity in the basal lamina. ***ii***, Removal of the crosshair allows visualization of the varicosity (arrowhead), which has a diameter of 0.47 µm. Higher magnification images of the white and magenta boxed areas are further examined in ***D*** and ***F***, respectively, in order to follow the path of the fiber. ***D***, Magnified view in three orientations of the investigated varicosity to better visualize the varicosity in relation to the vascular wall. ***i***, GRP, collagen, lectin, and DAPI staining are merged to show that the varicosity is in the basal lamina. ***ii***, Removal of collagen shows the varicosity lying outside the territory of the endothelium. Arrowheads point to the location of the varicosity as in ***C***. ***E***, Cartoon provides traces of key elements in ***D***. ***F***, Serial optical sections show the pathway of a GRP fiber (arrows) above (***i–iii***) and below (***v–x***) a varicosity (***iv***) of the boxed area in ***C*** as it enters and exits the basal lamina, leaving five visible varicosities in the BV wall. Top row, Merged images of GRP and BV show the path of the fiber. Bottom row, The GRP-only channel enhances visualization of the fiber. ***i***, ***ii***, A GRP fiber segment with varicosities gradually appear and (***iii–v***) traverse the basal lamina horizontally. ***vi–ix***, The other end of the fiber exits the basal lamina and (***x***) gradually disappears. The arrowhead in ***iv*** serves as a location marker and points to the varicosity seen in ***C*** and ***D***. GRP (red), gastrin-releasing peptide; remaining color coding and abbreviations as in Figure 1. For ***B***, $z = 17.1$ µm; for ***C***, ***D***, and ***F***, $z = 0.1$ µm; ***F*** was taken from every fourth section in the z stack.

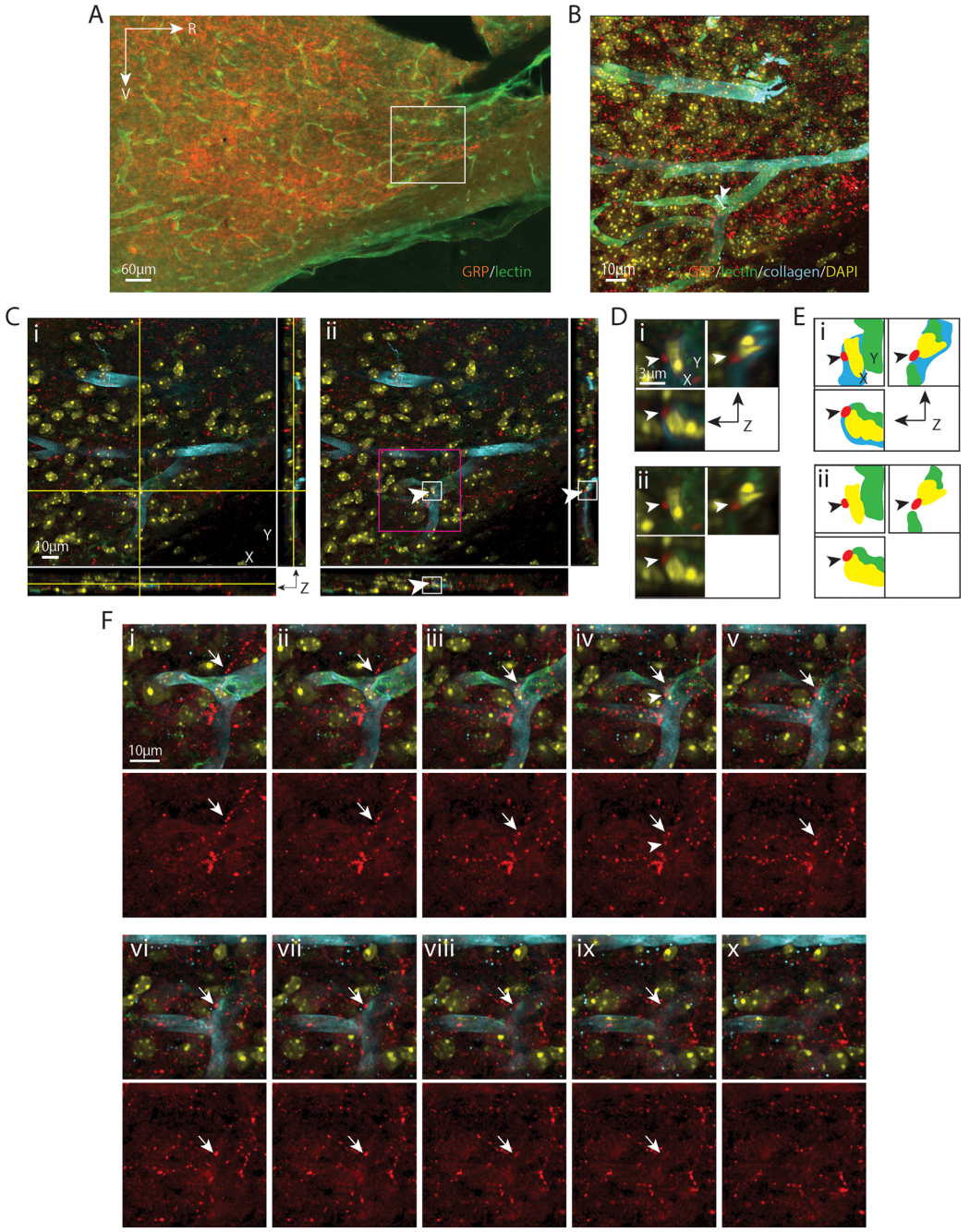


Figure 6. GRP varicosity contacting a pericyte nucleus. ***A***, EDF image of the SCN in sagittal orientation, labeled with GRP for SCN and lectin for endothelium. The boxed area is further imaged with a confocal microscope in ***B–F***. ***B***, Maximum intensity projection of confocal image of the boxed area in ***A*** with additional labels of basal lamina (collagen) and nuclei (DAPI). Numerous GRP fibers are seen coursing over the capillaries. The capillary segment (arrowhead) examined in the following panels has a diameter of 8.92 µm. ***C***, A GRP-positive varicosity, shown in all three orientations, contacts DAPI in an optical section taken from ***B***. ***i***, The crosshair denotes the location of varicosity contacting the DAPI-labeled cell nucleus in the basal lamina. ***ii***, The crosshair is removed to enhance visualization of the varicosity (arrowhead), which has a diameter of 0.72 µm. Higher magnification images of the white and magenta boxed areas are further examined in ***D*** and ***F***, respectively, in order to follow the path of the fiber. ***D***, Magnified view in three orientations of the varicosity contacting the cell nucleus to better visualize the varicosity in relation to the vascular wall. ***i***, GRP, collagen, lectin, and DAPI staining are merged to show that the varicosity is in the basal lamina. ***ii***, Removing collagen shows left half of the cell nucleus contacted by the GRP-positive varicosity is not covered by collagen and its right aspect is covered by lectin, indicating that the cell is localized within the basal lamina. The tip of the varicosity touches the nucleus on all three orientations, and its main body is localized in the basal lamina. Arrowheads point to the location of the varicosity as in ***C***. ***E***, Cartoon provides traces of key elements in ***D***. ***F***, Serial sections indicate the pathway of a GRP fiber (arrows) coursing above (***i–iii***) a varicosity (***iv***) that terminates on a cell in the basal lamina (***v–x***). Top row: Merged images of GRP and BV show the path of the fiber. Bottom row: The GRP-only channel enhances visualization of the fiber. ***i–iii***, A GRP fiber reaches the capillary from the 1 o'clock direction and enters the basal lamina. ***iv–vi***, The varicosity contacts a DAPI-labeled cell nucleus surrounded by collagen. ***vii–x***, The staining of the varicosity and the cell where the varicosity resides gradually disappear together. Arrows point to the fiber terminating on the basal lamina cell. The arrowhead in ***iv*** points to the same varicosity as in ***C*** and ***D***. Color coding and abbreviations as in Figure 4. For ***B***, $z = 18.1$ µm; for ***C***, ***D***, and ***F***, $z = 0.1$ µm; ***F*** was taken from every fourth section across the z stack.

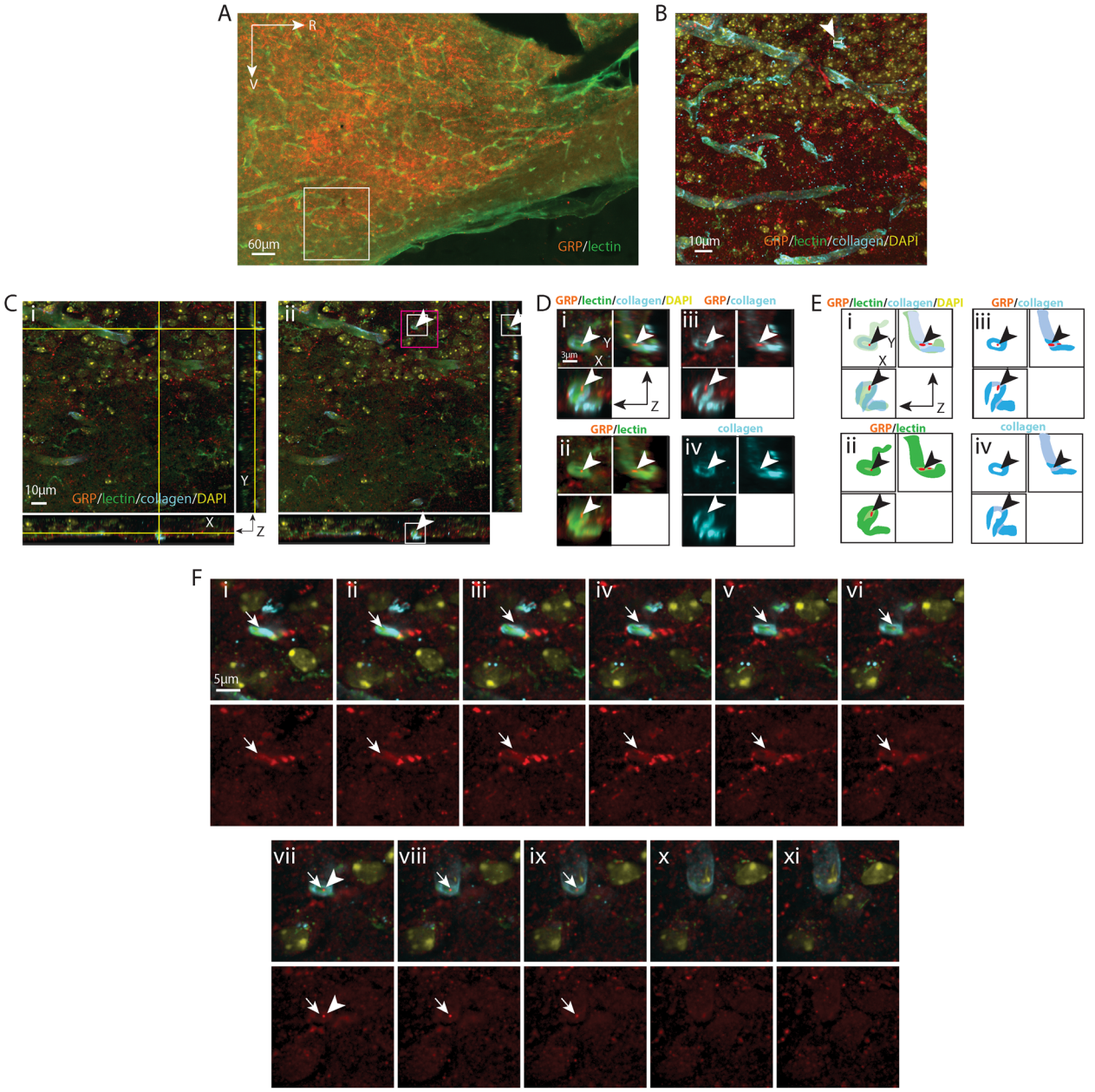


Figure 7. GRP varicosity lying in the capillary endothelium. ***A***, EDF image of the SCN in sagittal orientation, labeled with GRP for SCN and lectin for endothelium. The boxed area is further imaged with a confocal microscope in ***B–F***. ***B***, Maximum intensity projection of confocal image of the boxed area in ***A*** with additional labels of for basal lamina (collagen) and nuclei (DAPI). GRP fibers are seen intertwined with capillaries. The capillary segment (arrowhead) examined in the following panels has a diameter of 7.90 µm. ***C***, A GRP varicosity in the endothelium is shown in all three orientations in an optical section taken from ***B***. ***i***, The crosshair denotes the location of the varicosity in the endothelium. ***ii***, Removal of the crosshair allows better visualization of the varicosity (arrowheads), which has a diameter of 0.46 µm. Higher magnification images of the white and magenta boxed areas are further examined in ***D*** and ***F*** respectively, in order to follow the path of the fiber. ***D***, Magnified view in all three orientations allows visualization of the varicosity in relation to the vascular endothelium. ***i***, GRP, collagen, and lectin staining are merged to show the varicosity (arrowheads) in the endothelium. ***ii***, collagen and lectin channels are merged showing that a GRP varicosity lies in the gap of lectin staining (arrowheads). ***iii***, the GRP and collagen channels are merged showing that the GRP varicosity is not localized to the basal lamina as it lies in a "cavity" (arrowheads) lacking collagen staining. ***iv***, The collagen-only channel allows better visualize the cavity (arrowheads) in the basal lamina. ***E***, Cartoon provides traces of key elements in ***D***. ***F***, Serial sections indicate the pathway of a GRP fiber (arrows) above (***i–vi***) and below (***viii–xi***) a varicosity (***vii***) which terminates in the endothelium. Top row, Merged images of GRP and BV show the pathway of the fiber. Bottom row: The GRP-only channel allows better visualization of the fiber. ***i–v***, The varicosities of a GRP fiber segment gradually appear and surround a capillary vessel. ***vi–viii***, A varicosity on this fiber is seen in the endothelium. ***ix–xi***, The varicosity gradually disappears. The arrowhead in ***vii*** serves as a location marker and points to the varicosity seen in ***C***, ***D***. Color coding and abbreviations as in Figure 4. For ***B***, $z = 21.1$ µm; for ***C***, ***D***, and ***E***, $z = 0.1$ µm; ***F*** was taken from every fourth section across the z stack.

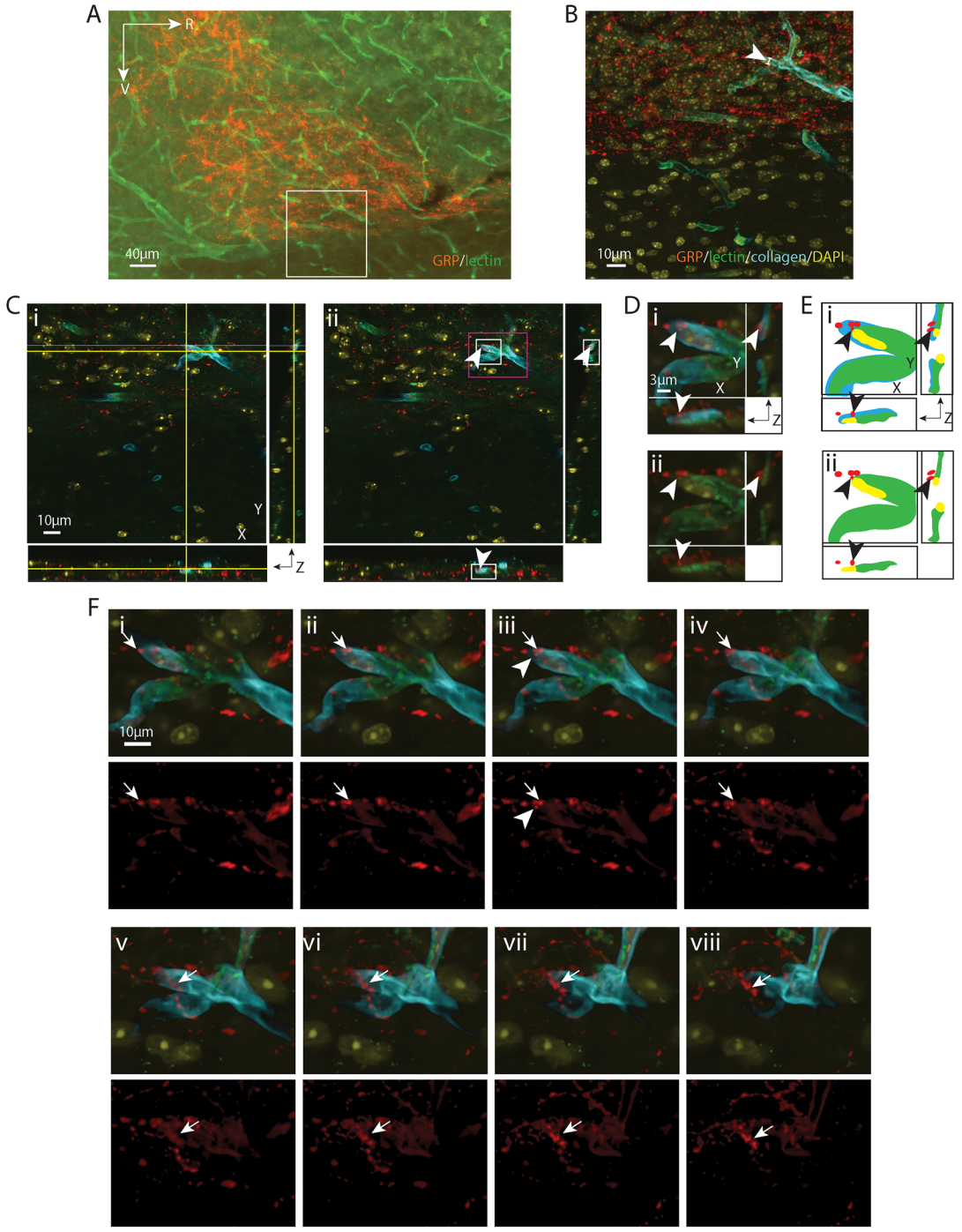


Figure 8. VIP varicosity lying in the capillary basal lamina matrix. ***A***, EDF image of the SCN in sagittal orientation, labeled with VIP for SCN and lectin for endothelium. The boxed area is further imaged with a confocal microscope in ***B–F***. ***B***, Maximum intensity projection of confocal image of the boxed area in ***A*** with additional labels of for basal lamina (collagen) and nuclei (DAPI). VIP-positive fibers are seen coursing over the BV. The capillary segment (arrowhead) examined in the following panels has a diameter of 5.57 µm. ***C***, A VIP-positive varicosity lying in the basal lamina, shown in all three orientations, in an optical section taken from ***B***. ***i***, The crosshair denotes the varicosity in the basal lamina. ***ii***, Removal of the crosshair enables better visualization of the varicosity (arrowhead), which has a diameter of 0.57 µm. Higher magnification images of the white and magenta boxed areas are further examined in ***D*** and ***F*** respectively, in order to follow the path of the fiber. ***D***, Magnified view in three orientations allows visualization of the varicosity in relation to the basal lamina and vascular wall. ***i***, VIP, collagen, lectin, and DAPI staining are merged to show that the varicosity is in the basal lamina. ***ii***, Removal of collagen shows the varicosity lying outside the territory of the endothelium. Arrowheads point to the location of the varicosity as in ***C***. ***E***, Cartoon provides traces of key elements in ***D***. ***F***, Serial optical sections show the pathway of a VIP fiber (arrows) above (***i***, ***ii***) and below (***iv–viii***) a varicosity (***iii***) of the boxed area in ***C*** as it enters and exits the basal lamina. Top row: Merged images of VIP and BV display the path of the fiber. Bottom row: The VIP-only channel allows better visualization of the fiber. ***i***, ***ii***, A VIP fiber reaches the BV. ***iii***, ***iv***, The fiber branches and the varicositie senter the BV basal lamina. ***v–viii***, The branch further extends and exits the BV wall. The arrowhead in ***iii*** serves as a location marker and points to the varicosity seen in ***C***, ***D***. Color coding and abbreviations: VIP, red; VIP, vasoactive intestinal peptide; the remaining are as in Figure 1. For ***B***, $z = 23.1$ µm; for ***C***, ***D***, and ***F***, $z = 0.1$ µm; ***F*** was taken from every fourth section across the *z* stack.

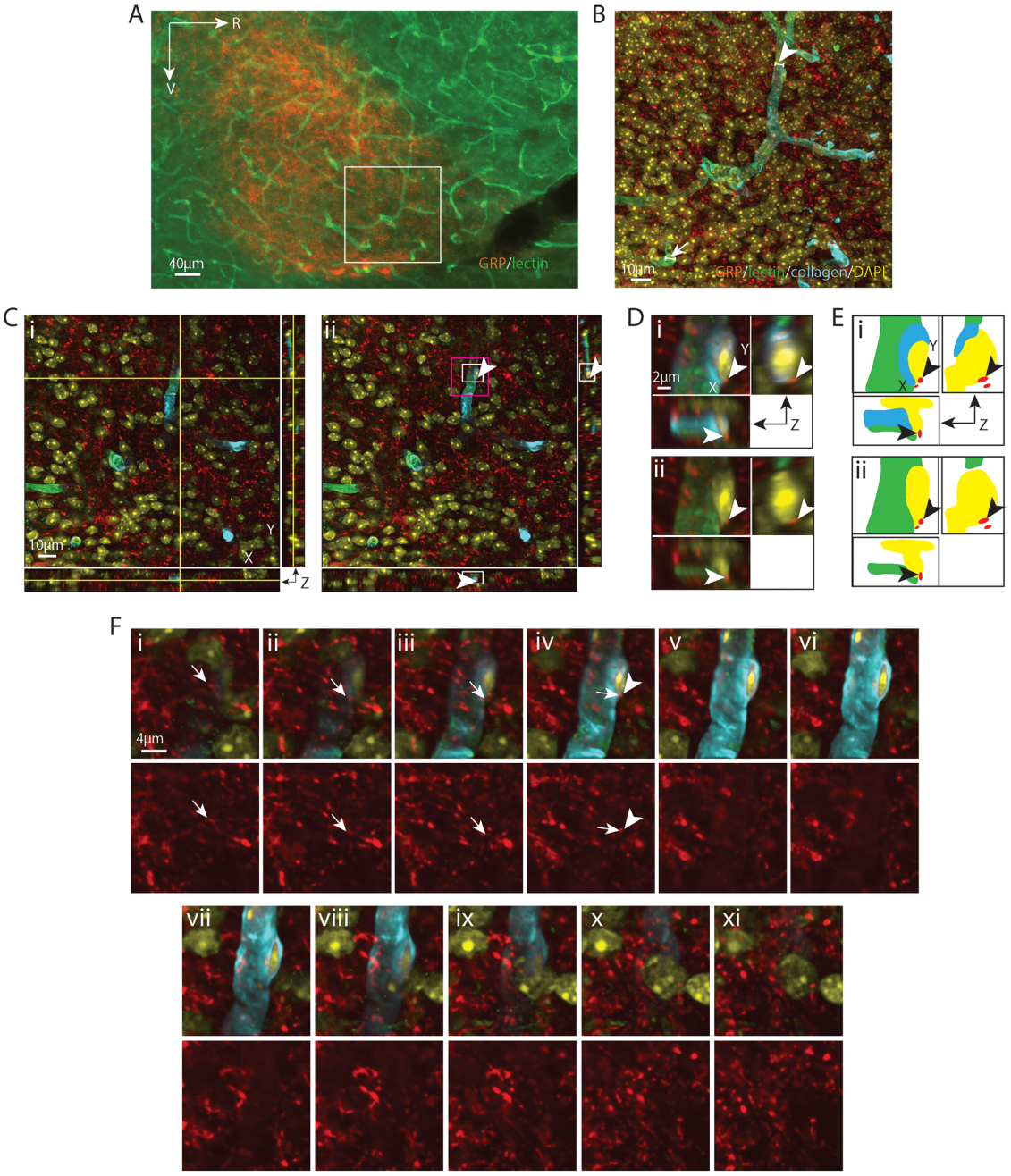


Figure 9. VIP varicosity contacting a pericyte nucleus. ***A***, EDF image of the SCN in sagittal orientation, labeled with VIP for SCN and lectin for endothelium. The boxed area is further imaged with a confocal microscope in ***B–F***. ***B***, Maximum intensity projection of confocal image of the boxed area in ***A*** with additional labels of basal lamina (collagen) and nuclei (DAPI). VIP fibers are seen coursing over the capillaries. The capillary segment examined in Figure 8 (arrowhead) has a diameter of 6.05 µm. The capillary segment examined Figure 9 (arrow) has a diameter of 4.39 µm. ***C***, A VIP-positive varicosity, shown in all three orientations, contacts DAPI in an optical section taken from ***B***. ***i***, The crosshair denotes the location of varicosity contacting the DAPI-labeled cell nucleus in the basal lamina. ***ii***, Removal of the crosshair enables better visualization of the varicosity (arrowhead), which has a diameter of 0.53 µm. The varicosity touches a cell nucleus localized in the capillary wall, protruding from the trunk. Higher magnification images of the white and magenta boxed areas are further examined in ***D*** and ***F***, respectively, in order to follow the path of the fiber. ***D***, Magnified view in three orientations allows visualization of the varicosity in the basal lamina. ***i***, VIP, collagen, lectin and DAPI staining are merged to show the varicosity contacting the nucleus. Half of the perimeter of the nucleus borders the endothelium in the *xy* orientation, but in the *xz* and *yz* orientations, the nucleus is separated from the endothelium by the basal lamina. ***ii***, Removal of collagen channel shows that the right half of the cell nucleus contacted by the VIP-positive varicosity is not covered by collagen and that its left aspect is covered by lectin. Arrowheads point to the location of the varicosity as in ***C***. ***E***, Cartoon provides traces of key elements in ***D***. ***F***, Serial sections indicate the pathway of a VIP fiber (arrows) coursing above (***i–iii***) a varicosity (***iv***) that terminates on a cell in the basal lamina (***vi–xi***). Top row, Merged images of VIP and BV show the path of the fiber. Bottom row, The VIP-only channel enhances visualization of the fiber. ***i–iii***, A VIP fiber appears and reaches the capillary and enters the basal lamina. ***iv***, The terminal of VIP fiber touches a DAPI-labeled cell surrounded by collagen whereas the fiber entry point is not covered by collagen. ***v–vii***, The varicosity disappears, and the cell is fully wrapped by the collagen. ***viii–xi***, The blood vessel gradually disappears. The arrowhead in ***iv*** serves as a location marker and points to the varicosity seen in ***C***, ***D***. Color coding and abbreviations as in Figure 7. For ***B***, $z = 14.1$ µm; for ***C***, ***D***, and ***E***, $z = 0.15$ µm; ***D*** was taken from every fourth section across the *z* stack.

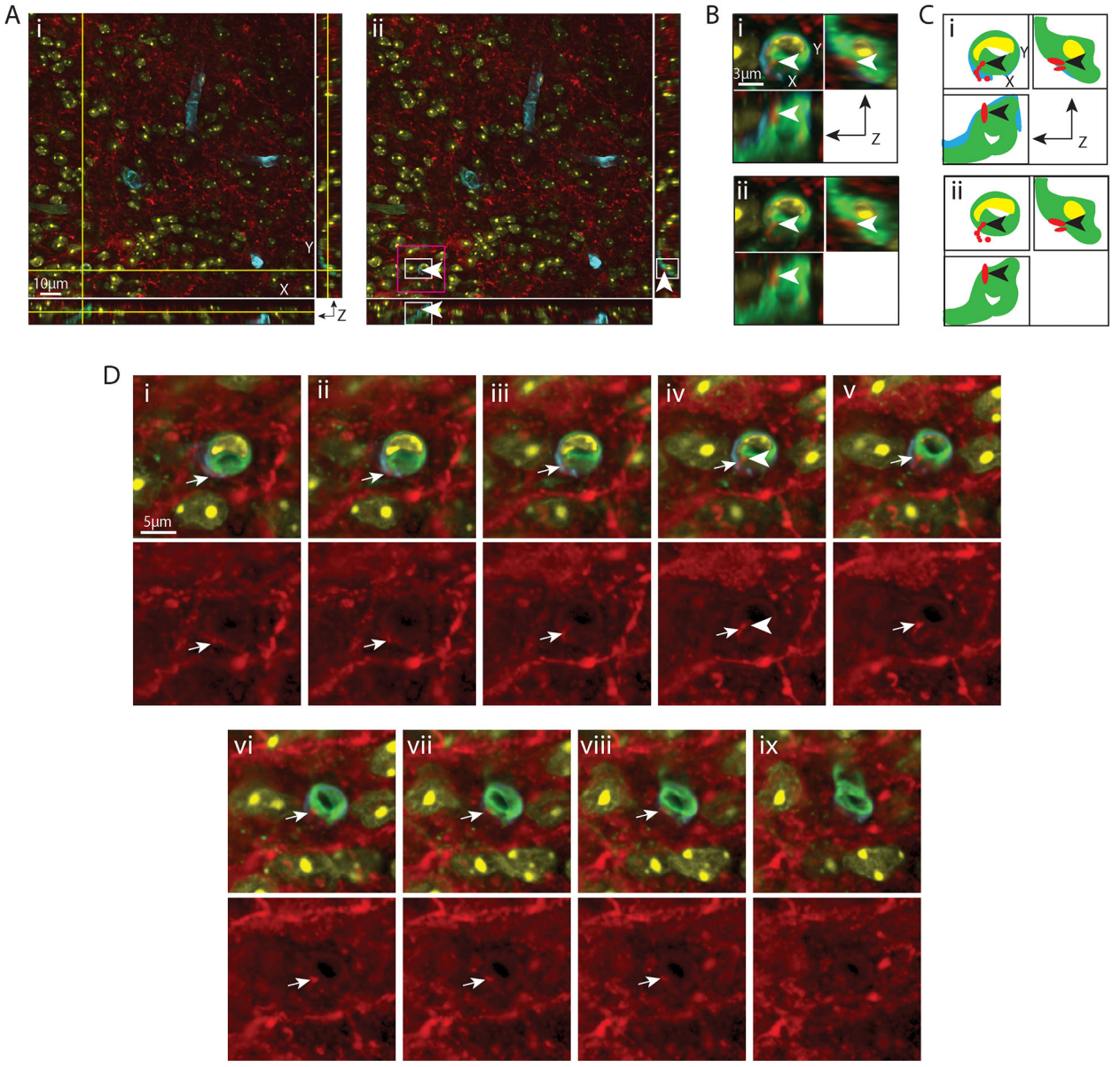


Figure 10. VIP fibers varicosity lying in the capillary endothelium. ***A***, A VIP varicosity in the endothelium is shown in all three orientations in an optical section taken from Figure 8*B*. ***i***, The crosshair denotes the location of the varicosity in the endothelium. ***ii***, Removal of the crosshair allows better visualization of the varicosity (arrowheads), which has a diameter of 0.65 µm. Higher magnification images of the white and magenta boxed areas are further examined in ***B*** and ***D***, respectively, in order to follow the path of the fiber. ***B***, Magnified view of the varicosity in all three orientations allows visualization of the varicosity in relation to the vascular endothelium. ***i***, VIP, collagen, lectin, and DAPI staining are merged to show that the varicosity is in the endothelium. ***ii***, Removal of collagen to show the varicosity is not localized in the basal lamina. Arrowheads point to the location of the varicosity as in ***A***. ***C***, Cartoon provides traces of key elements in ***B***. ***D***, Serial sections indicate the pathway (***i–iii***) of a VIP fiber (arrows). The varicosity (***iv***) terminates in the endothelium (***v–ix***). Top row: Merged images of VIP and BV show the path of the fiber. Bottom row: The VIP-only channel enhances visualization of the fiber. ***i–iii***, A VIP fiber appears and reaches the basal lamina of a capillary from the 7 o'clock direction. ***iv–vi***, The terminal of VIP fiber further enters the endothelium. ***vi–ix***, The varicosity gradually disappears. The arrowhead in ***iv*** serves as a location marker and points to the varicosity seen in ***A*** and ***B***. Color coding and abbreviations as in Figure 7. For ***A***, ***B***, and ***D***, $z = 0.15$ µm; ***D*** was taken from every fourth section across the z stack.

end foot sheath which were occupied by cellular processes. The activity of astrocyte end feet in regulating components of the BBB is also highly regional and dynamic (Segarra et al., 2021; Díaz-Castro et al., 2023; Pociūtė et al., 2024). The current results and the broader literature support the possibility that while the majority of brain vasculature is covered by the astroglial end feet, this may not be the case for the entire vasculature surface. The present study raises the question of whether spaces between the end feet allow neuronal processes to access the vasculature wall.

The major findings of the present study are consistent with the accumulating evidence that vasoactive fibers innervate brain vasculature. In the SCN, we observed varicosity contacts over each region of the SCN (Fig. 1) of all three vasoactive

peptides that were examined. The distribution of these contacts seemed to be related to the density and location of the varicosities. The contacts of AVP varicosities with the capillaries were found mostly in the shell along the rostrocaudal extension of the SCN and were rarely found in the core. The VIP and GRP varicosities were found throughout the entire extent of SCN. We conjecture that AVP has greater functional importance in the dense shell capillaries, while GRP and VIP have a more general effect on the entire SCN vasculature. While the relationship of AVP, VIP, and GRP varicosities to the vasculature of the SCN has never been examined, the present results are consistent with prior findings in the literature in other brain regions. For AVP, brain microvessel innervation by neurons has been reported in rats (Jójárt et al., 1984). Based on peroxidase-antiperoxidase immunocytochemistry and EM, they reported that AVP-positive elements establish direct contacts with the basal lamina of the endothelium or of a pericyte associated with the capillary bed. Furthermore, the results demonstrated that the AVP-containing neural processes that contact BVs are mainly dendrites, suggesting that the vasopressinergic neuronal elements can directly innervate brain microvessels. VIP has been reported in the discontinuities of astrocyte end feet and in close contact with the basal lamina of microvessels in the rat cortex (Paspalas and Papadopoulos, 1998). In addition, there is substantial VIP innervation of brain arteries in rats and mice (Lorén et al., 1979; Eckenstein and Baughman, 1984; Suzuki et al., 1988). While there are few studies of this peptide, GRP terminals reportedly innervate pial vessels in cats, guinea pigs, rats, and mice (Uddman et al., 1983). Additionally, several studies point to capillary innervation by other transmitters or modulators in extra-SCN brain regions. Innervation of capillaries by local neurons has been demonstrated in the cat hypothalamus (Rennels et al., 1983). Such contacts are not limited to vasoactive peptides; there is ultrastructural evidence of central monoaminergic innervation of BVs in the paraventricular nucleus of the hypothalamus (Larsson et al., 1976; Swanson et al., 1977). Finally, in the hepatic portal system, there is ultrastructural evidence of substance P and VIP innervation of BV, which are known to play a role in the modulation of rhythmic contractions (Barja and Mathison, 2008).

A caveat in this study is that fixation and preparation can have huge effects on tissue morphology. Collapse of perivascular spaces upon death of the animal and fixation of the tissue have been documented (Mestre et al., 2018). Projections to the basal lamina of the capillaries may reach perivascular spaces and could implicate glymphatic movement (Silver et al., 2025). This interesting possibility requires functional/dynamic studies in living animals. Additionally, the present results rest on confocal imaging methods, and further multimodal approaches will be essential for studying the structural organization and dynamic properties of neural–vascular communication systems. Greater resolution, in studies using nanoscale imaging techniques, EM, including scanning, transmission, and volume EM, will enable higher resolution visualization of the ultrastructure of fiber contacts with the neurovascular unit. Each technique, however, has distinct advantages and limitations. EM is limited by a relatively small field of view and restricted capacity for simultaneous identification of multiple proteins (Malatesta, 2021; Peddie et al., 2022). Super-resolution microscopy techniques beyond confocal imaging, which overcome the diffraction limit, also offer powerful tools for studying vasoactive fiber contacts with the vasculature. Although these methods enable visualization of multiple proteins and can be applied to study the activities of vasoactive fibers in vivo, they rely on indirect signals from fluorescent labels rather than direct structural visualization. In addition, the high cost of implementing super-resolution microscopy has hindered its widespread application (Schermelleh et al., 2019; Fuhrmann et al., 2022).

While it has not been studied directly, it is possible that the vasoactive peptides of the SCN act on the receptors in the vasculature. AVP receptors are widely distributed in the brain BV (Ostrowski et al., 1994). Upon brain injury, significantly increased AVP V_{1a} receptors localized on the vascular endothelium increase BBB permeability (Szmydynger-Chodobska et al., 2004). In Brattleboro rats, vasopressin binding sites show in the brain BVs in AVP-implanted animals but not in water-filled controls (van Zwieten et al., 1988). Furthermore, the staining was dose-dependent. The authors note that AVP binding on endothelial and pericyte cells points to a role in alteration of BBB permeability and involvement of pericytes in regulating blood flow in small vessels. While the evidence in Brattleboro rats is interesting but requires cautious interpretation, given their diabetic state and severely compromised physiology. VIP receptors have also been reported in brain BVs, and they are expressed exclusively in smooth muscle cells, not in the endothelium (Erdling et al., 2013). The same study also reported that only abluminal application of VIP could cause vascular relaxation. In an ischemia model with middle cerebral artery occlusion, intraventricularly administered VIP significantly reduced BBB permeability, shown by Evans Blue extravasation (Yang et al., 2022). To our knowledge, there is no report about the effect of GRP on brain vasculature. The present results point to the importance of exploring how SCN-derived neuropeptides regulate local hemodynamics and whether the hemodynamic changes impact the circadian regulation functions of the brain's clock.

There is limited information available on the localization of intra-SCN receptors for these vasoactive peptides. The mRNA of AVP receptors V1a and V1b is present in the SCN (Bedont et al., 2018). V1a shows strong expression in the central SCN and has a clear diurnal rhythm, peaking in the middle of the dark phase. It also displays differential expression along the rostrocaudal axis, with higher expression in the caudal SCN and lower in the rostral region when standardized to the entire SCN. In contrast, V1b is expressed at lower levels in the central SCN and is not rhythmic. There are two types of VIP receptors in the central nervous system, termed VPAC1 and VPAC2. Within the SCN, VPAC1 is not detected in SCN neurons but is extensively expressed in the vasculature (Stangerup and Hannibal, 2020; Fig. 1*D*). In contrast, VPAC2 is broadly distributed throughout the SCN, with higher expression in the dorsal region than in the ventral area (An et al., 2012). The same study also reported that approximately 94.4% of cultured SCN cells express VPAC2, primarily localized

to dendrites and cell bodies. In another study, VPAC2 mRNA was identified in nearly all AVP neurons and 41% of VIP neurons (Kalamatianos et al., 2004). VPAC2 mRNA also exhibits diurnal rhythmicity, reaching a trough in the middle of the light phase (Kalló et al., 2004). The GRP receptor is likewise expressed in the SCN. Karatsoreos et al. (2006) demonstrated that GRP receptors are distributed across the rostrocaudal extent of the nucleus, with localization predominantly in the dorsal and medial SCN and lower expression in the ventrolateral region. They further reported that GRP receptor binding activity peaks at the onset of the dark phase, paralleling the oscillatory pattern of GRP receptor protein levels in the SCN. Finally, to the best of our knowledge, there are no data on whether there are receptors for AVP or GRP within the SCN vasculature.

The SCN–OVLT portal venules constitute a possible pathway for delivering peptides of SCN origin to the OVLT. Of the three vasoactive peptides studied here, AVP is the most likely to be involved in the SCN–OVLT portal communications. The portal vessels originate at the rostral shell of the SCN, a region rich in AVP. Single-cell RT-PCR revealed AVP V1a receptors in OVLT neurons (Gizowski et al., 2016), implying that OVLT is a target for this peptide. In addition, there are carrier-mediated systems transporting AVP from the brain to the blood (Banks et al., 1987). Although it has not been examined in the SCN, in other brain regions, peptides can enter the vasculature by efflux transport (Cox et al., 2023) and by transcytosis (Ayloo and Gu, 2019).

While the present study is strictly anatomical, it provides a solid foundation for future mechanistic work. The results suggest that varicosities of all three vasoactive peptides are found in the SCN vascular basal lamina and endothelium, pointing to the possibility that they may breach the BBB. This finding opens the opportunity for studying local vascular regulation within the nucleus. Given the portal connection between SCN and OVLT, these vasoactive peptides are positioned to modulate SCN hemodynamics and modulate diffusible signal efficacy. Possibly, neurosecretions relayed from the SCN to the OVLT and thence to other brain regions thereby provide for global signaling supporting daily rhythms (Silver et al., 2025).

References

Abbott NJ, Rönnbäck L, Hansson E (2006) Astrocyte–endothelial interactions at the blood–brain barrier. Nat Rev Neurosci 7:41–53.

Abrahamson EE, Moore RY (2001) Suprachiasmatic nucleus in the mouse: retinal innervation, intrinsic organization and efferent projections. Brain Res 916:172–191.

Al-Huthaifi AM, Radman BA, Al-Alawi AA, Mahmood F, Liu T-B (2024) Mechanisms and virulence factors of *Cryptococcus neoformans* dissemination to the central nervous system. J Fungi 10:586.

Ambach G, Palkovits M (1975) Blood supply of the rat hypothalamus. III. Anterior region of the hypothalamus (nucleus suprachiasmatis, nucleus hypothalamicus anterior, nucleus periventricularis). Acta Morphol Acad Sci Hung 23:21–49.

An S, Tsai C, Ronecker J, Bayly A, Herzog ED (2012) Spatiotemporal distribution of vasoactive intestinal polypeptide receptor 2 in mouse suprachiasmatic nucleus. J Comp Neurol 520:2730–2741.

Armulik A, et al. (2010) Pericytes regulate the blood–brain barrier. Nature 468:557–561.

Ayloo S, Gu C (2019) Transcytosis at the blood–brain barrier. Curr Opin Neurobiol 57:32–38.

Bai W, Zhou Y-G (2017) Homeostasis of the intraparenchymal-blood glutamate concentration gradient: maintenance, imbalance, and regulation. Front Mol Neurosci 10:400.

Banks WA (2016) From blood–brain barrier to blood–brain interface: new opportunities for CNS drug delivery. Nat Rev Drug Discov 15:275–292.

Banks WA, Kastin AJ, Horvath A, Michals EA (1987) Carrier-mediated transport of vasorpressin across the blood-brain barrier of the mouse. J Neurosci Res 18:326–332.

Barja F, Mathison R (2008) Adrenergic and peptidergic (substance P and vasoactive intestinal polypeptide) innervation of the rat portal vein. Blood Vessels 19:263–272.

Bedont JL, Rohr KE, Bathini A, Hattar S, Blackshaw S, Sehgal A, Evans JA (2018) Asymmetric vasopressin signaling spatially organizes the master circadian clock. J Comp Neurol 526:2048–2067.

Bertossi M, Virgintino D, Maiorano E, Occhiogrosso M, Roncali L (1997) Ultrastructural and morphometric investigation of human brain capillaries in normal and peritumoral tissues. Ultrastruct Pathol 21:41–49.

Clive S, Jodrell D, Webb D (2001) Gastrin-releasing peptide is a potent vasodilator in humans. Clin Pharmacol Ther 69:252–259.

Cox B, Nicolaï J, Williamson B (2023) The role of the efflux transporter, P-glycoprotein, at the blood–brain barrier in drug discovery. Biopharm Drug Dispos 44:113–126.

Díaz-Castro B, Robel S, Mishra A (2023) Astrocyte endfeet in brain function and pathology: open questions. Annu Rev Neurosci 46:101–121.

Eckenstein F, Baughman RW (1984) Two types of cholinergic innervation in cortex, one co-localized with vasoactive intestinal polypeptide. Nature 309:153–155.

Erdling A, Sheykhzade M, Maddahi A, Bari F, Edvinsson L (2013) VIP/PACAP receptors in cerebral arteries of rat: characterization, localization and relation to intracellular calcium. Neuropeptides 47:85–92.

Fuhrmann M, Gockel N, Arizono M, Dembitskaya Y, Nägerl UV, Pennacchietti F, Damenti M, Testa I, Willig KI (2022) Super-resolution microscopy opens new doors to life at the nanoscale. J Neurosci 42:8488.

Gizowski C, Zaelzer C, Bourque CW (2016) Clock-driven vasopressin neurotransmission mediates anticipatory thirst prior to sleep. Nature 537:685–688.

Goadsby PJ, MacDonald GJ (1985) Extracranial vasodilatation mediated by vasoactive intestinal polypeptide (VIP). Brain Res 329:285–288.

Goldsmith SR (1987) Vasopressin as vasopressor. Am J Med 82:1213–1219.

Haim LB, Rowitch DH (2017) Functional diversity of astrocytes in neural circuit regulation. Nat Rev Neurosci 18:31–41.

Härtig W, Reichenbach A, Voigt C, Boltze J, Bulavina L, Schuhmann MU, Seeger J, Schusser GF, Freytag C, Grosche J (2009) Triple fluorescence labelling of neuronal, glial and vascular markers revealing pathological alterations in various animal models. J Chem Neuroanat 37:128–138.

Jacomy H, Burlet A, Bosler O (1999) Vasoactive intestinal peptide neurons as synaptic targets for vasopressin neurons in the suprachiasmatic nucleus. Double-label immunocytochemical demonstration in the rat. Neuroscience 88:859–870.

Jójárt I, Joó F, Siklós L, László FA (1984) Immunoelectronhisto chemical evidence for innervation of brain microvessels by vasopressin-immunoreactive neurons in the rat. Neurosci Lett 51:259–264.

Kalamatianos T, Kalló I, Coen CW (2004) Ageing and the diurnal expression of the mRNAs for vasopressin and for the V1a and V1b vasopressin receptors in the suprachiasmatic nucleus of male rats. J Neuroendocrinol 16:493–501.
Kalló I, Kalamatianos T, Piggins HD, Coen CW (2004) Ageing and the diurnal expression of mRNAs for vasoactive intestinal peptide and for the VPAC2 and PAC1 receptors in the suprachiasmatic nucleus of male rats. J Neuroendocrinol 16:758–766.
Karatsoreos IN, Romeo RD, McEwen BS, Silver R (2006) Diurnal regulation of the gastrin-releasing peptide receptor in the mouse circadian clock. Eur J Neurosci 23:1047–1053.
Larsson L-I, Edvinsson L, Fahrenkrug J, Håkanson R, Owman C, Schaffalitzky de Muckadell O, Sundler F (1976) Immunohisto chemical localization of a vasodilatory polypeptide (VIP) in cerebrovascular nerves. Brain Res 113:400–404.
Lokshin M, LeSauter J, Silver R (2015) Selective distribution of retinal input to mouse SCN revealed in analysis of sagittal sections. J Biol Rhythms 30:251–257.
Lorén I, Emson PC, Fahrenkrug J, Björklund A, Alumets J, HåkansonR, Sundler F (1979) Distribution of vasoactive intestinal polypeptide in the rat and mouse brain. Neuroscience 4:1953–1976.
Malatesta M (2021) Transmission electron microscopy as a powerful tool to investigate the interaction of nanoparticles with subcellular structures. Int J Mol Sci 22:12789.
Mathiisen TM, Lehre KP, Danbolt NC, Ottersen OP (2010) The perivascular astroglial sheath provides a complete covering of the brain microvessels: an electron microscopic 3D reconstruction. Glia 58:1094–1103.
Maywood ES, Chesham JE, O'Brien JA, Hastings MH (2011) A diversity of paracrine signals sustains molecular circadian cycling in suprachiasmatic nucleus circuits. Proc Natl Acad Sci U S A 108:14306–14311.
Mestre H, Tithof J, Du T, Song W, Peng W, Sweeney AM, Olveda G, Thomas JH, Nedergaard M, Kelley DH (2018) Flow of cerebrospinal fluid is driven by arterial pulsations and is reduced in hypertension. Nat Commun 9:4878.
Meyer-Bernstein EL, Jetton AE, Matsumoto S, Markuns JF, Lehman MN, Bittman EL (1999) Effects of suprachiasmatic transplants on circadian rhythms of neuroendocrine function in golden hamsters. Endocrinology 140:207–218. ; **This work was supported by NIH Grants MH-44132, KO2-MH-00914, and F32-HD-07673. A preliminary report of this research was presented at the 23rd Annual Meeting of the Society for Neuroscience (Neurosci Abstr 19:236.17, 1993).
Michalski D, et al. (2020) Increased immunosignals of collagen IV and fibronectin indicate ischemic consequences for the neurovascular matrix adhesion zone in various animal models and human stroke tissue. Front Physiol 11:575598.
Moore RY, Speh JC, Leak RK (2002) Suprachiasmatic nucleus organization. Cell Tissue Res 309:89–98.
Moore RY, Silver R (1998) Suprachiasmatic nucleus organization. Chronobiol Int 15:475–487.
Ono D, Weaver DR, Hastings MH, Honma K-I, Honma S, Silver R (2024) The suprachiasmatic nucleus at 50: looking back, then looking forward. J Biol Rhythms 39:135–165.
Ostrowski NL, Lolait SJ, Young WS 3rd (1994) Cellular localization of vasopressin V1a receptor messenger ribonucleic acid in adult male rat brain, pineal, and brain vasculature. Endocrinology 135:1511–1528.
Pardridge WM (2002) Drug and gene delivery to the brain: the vascular route. Neuron 36:555–558.
Paspalas CD, Papadopoulos GC (1998) Ultrastructural evidence for combined action of noradrenaline and vasoactive intestinal polypeptide upon neurons, astrocytes, and blood vessels of the rat cerebral cortex. Brain Res Bull 45:247–259.
Peddie CJ, et al. (2022) Volume electron microscopy. Nat Rev Methods Primers 2:51.
Pociūtė A, Pivoriūnas A, Verkhratsky A (2024) Astrocytes dynamically regulate the blood-brain barrier in the healthy brain. Neural Regen Res 19:709–710.
Popa G, Fielding U (1930) The vascular link between the pituitary and the hypothalamus. Lancet 216:238–240.
Rennels ML, Gregory TF, Fujimoto K (1983) Innervation of capillaries by local neurons in the cat hypothalamus: a light microscopic study with horseradish peroxidase. J Cereb Blood Flow Metab 3:535–542.
Roy RK, Yao Y, Green IK, Aitken AV, Biancardi VC, Silver R, SternJE (2024) Blood flows from the SCN toward the OVLT within a new brain vascular portal pathway. Sci Adv 10: eadn8350.
Schermelleh L, Ferrand A, Huser T, Eggeling C, Sauer M, Biehlmaier O, Drummen GPC (2019) Super-resolution microscopy demystified. Nat Cell Biol 21:72–84.
Segarra M, Aburto MR, Acker-Palmer A (2021) Blood–brain barrier dynamics to maintain brain homeostasis. Trends Neurosci 44:393–405.
Silver R, LeSauter J, Tresco PA, Lehman MN (1996) A diffusible coupling signal from the transplanted suprachiasmatic nucleus controlling circadian locomotor rhythms. Nature 382:810–813.
Silver R, Yao Y, Myung J (2025) Global clock coordination by the brain clock in the suprachiasmatic nucleus through relay and amplification of diffusible and neural signaling. Eur J Neurosci 61:e70097.
Stangerup I, Hannibal J (2020) Localization of vasoactive intestinal polypeptide receptor 1 (VPAC1) in hypothalamic neuroendocrine oxytocin neurons; a potential role in circadian prolactin secretion. Front Neuroanat 14:579466.
Stefanovic B, Hutchinson E, Yakovleva V, Schram V, Russell JT, Belluscio L, Koretsky AP, Silva AC (2008) Functional reactivity of cerebral capillaries. J Cereb Blood Flow Metab 28:961–972.
Suzuki N, Hardebo JE, Owman C (1988) Origins and pathways of cerebrovascular vasoactive intestinal polypeptide-positive nerves in rat. J Cereb Blood Flow Metab 8:697–712.
Swanson LW, Connelly MA, Hartman BK (1977) Ultrastructural evidence for central monoaminergic innervation of blood vessels in the paraventricular nucleus of the hypothalamus. Brain Res 136:166–173.
Szmydynger-Chodobska J, Chung I, Koźniewska E, Tran B, Harrington FJ, Duncan JA, Chodobski A (2004) Increased expression of vasopressin V1a receptors after traumatic brain injury. J Neurotrauma 21:1090–1102.
Tamada Y, Tanaka M, Munekawa K, Hayashi S, Okamura H, Kubo T, Hisa Y, Ibata Y (1998) Neuron–glia interaction in the suprachiasmatic nucleus: a double labeling light and electron microscopic immunocytochemical study in the rat. Brain Res Bull 45:281–287.
Taub A, Carbajal Y, Rimu K, Holt R, Yao Y, Hernandez AL, LeSauter J, Silver R (2021) Arginine vasopressin-containing neurons of the suprachiasmatic nucleus project to CSF. eNeuro 8: ENEURO.0363-20.2021.
Tousson E, Meissl H (2004) Suprachiasmatic nuclei grafts restore the circadian rhythm in the paraventricular nucleus of the hypothalamus. J Neurosci 24:2983.
Uddman R, Edvinsson L, Owman C, Sundler F (1983) Nerve fibres containing gastrin-releasing peptide around pial vessels. J Cereb Blood Flow Metab 3:386–390.
Ueda S, Kawata M, Sano Y (1983) Identification of serotonin- and vasopressin immunoreactivities in the suprachiasmatic nucleus of four mammalian species. Cell Tissue Res 234:237–248.
van Zwieten EJ, Ravid R, Swaab DF, Van de Woude T (1988) Immunocytochemically stained vasopressin binding sites on blood vessels in the rat brain. Brain Res 474:369–373.
Varadarajan S, Tajiri M, Jain R, Holt R, Ahmed Q, LeSauter J, Silver R (2018) Connectome of the suprachiasmatic nucleus: new evidence of the core-shell relationship. eNeuro 5:ENEURO.0205-18.2018.
Wu D, Chen Q, Chen X, Han F, Chen Z, Wang Y (2023) The blood–brain barrier: structure, regulation and drug delivery. Signal Transduct Target Ther 8:217.

Yang J, Yang C, Yang Y, Jia N, Sun Q (2022) Protection of vasoactive intestinal peptide on the blood-brain barrier dysfunction induced by focal cerebral ischemia in rats. J Stroke Cerebrovasc Dis 31:106160.

Yang Q, Wang H, Gao L, Ma D, Xiong Y, Ye T, Liu Y, Shen Z, Zhang X, Li W (Under review). Spatial transcriptomic reconstruction of human SCN reveals rewiring of neuropeptide signaling network. Available at SSRN 5336840.

Yao Y, Taub AB, LeSauter J, Silver R (2021) Identification of the suprachiasmatic nucleus venous portal system in the mammalian brain. Nat Commun 12:5643.

Yao Y, Green IK, Taub AB, Tazebay R, LeSauter J, Silver R (2023) Vasculature of the suprachiasmatic nucleus: pathways for diffusible output signals. J Biol Rhythms 38:571–585.

Zhao Y, Gan L, Ren L, Lin Y, Ma C, Lin X (2022) Factors influencing the blood-brain barrier permeability. Brain Res 1788:147937.